THE ASTROPHYSICAL JOURNAL, 456:305–315, 1996 January 1

DISCOVERY OF THREE RADIO PULSARS FROM AN X-RAY–SELECTED SAMPLE

ALEX ZEPKA, JAMES M. CORDES, AND IRA WASSERMAN
Department of Astronomy, Cornell University, Ithaca, NY 14853
AND
SCOTT C. LUNDGREN
Naval Research Laboratories
Received 1994 November 22; accepted 1995 July 11

ABSTRACT

We report the discovery of three radio pulsars (PSR J0631+10, J1843+20, and J1908+0457) in a search targeted at *Einstein* IPC X-ray sources. The fastest, J0631+10, has a period of 0.288 s and high period derivative ($\dot{P} = 104 \times 10^{-15}$ s s^{-1}) corresponding to a spin-down age of only 43 kyr. From 1400 MHz to 2380 MHz the radio spectrum is nearly flat, and the pulse profile is very symmetrical with four narrow components and shows a high degree of linear polarization (>70%). In contrast, the 430 MHz pulse profile is significantly broader and depolarized, which we argue is because of propagation effects. Besides the *Einstein* detection, we also found a faint X-ray source at the pulsar's location in a *ROSAT* PSPC exposure. A search for X-ray pulsations was not possible since fewer than 50 net counts are available from either data set. Because both X-ray detections fall in the shadow of their respective detector supporting ribs, the uncertainties in the spectral analysis and X-ray position are rather large, making the separations between pulsar and X-ray source ($\sim 1'$) still consistent with an association between the two. The dispersion measure (DM = 125.3 pc cm^{-3}) is the largest of any known pulsar in the Galactic anticenter and is likely to be due in part to an increase in the electron density associated with the star-forming region 3 Mon in the pulsar's foreground. Our analysis suggests that J0631+10 is interacting with (and possibly embedded inside) the dark cloud LDN 1605. In search for confirmation of its high-energy emission, we folded available *Compton Gamma-Ray Observatory* EGRET data at the pulsar's position and period, finding γ-ray modulations that have less than 1% probability of being generated by noise. The two other pulsars, J1843+20 and J1908+0457, are also close to their respective X-ray sources (separation $<2'$), but their small spin-down luminosities and large distances render them unlikely X-ray emitters.

Subject headings: pulsars: individual (PSR J0631+10, PSR J1843+20, PSR J1908+04) — radio continuum: stars — X-rays: stars

1. INTRODUCTION

Several strategies are followed in the searches for radio pulsars now being conducted, ranging from blind surveys of large regions of the sky to targeted searches of objects suspected of being neutron stars. In this paper, we discuss a search targeted toward a sample of X-ray sources that has led to the discovery of a young radio pulsar that we believe shows X-ray and possibly γ-ray emission.

The rationale for our survey was that radio pulsars may emit X-rays through a variety of mechanisms and that a targeted search of an X-ray–selected sample could yield high-sensitivity limits or detections of such sources.

There are many ways in which observable X-ray emission may arise in association with radio pulsars. Among the possibilities are the following:

1. Pulsed X-rays from the magnetosphere or surface of the neutron star. Young pulsars ($<10^4$ yr) like the Crab pulsar, B0540−69, and B1509−58, emit nonthermal X-rays via synchrotron or curvature radiation. Older objects ($<10^6$ yr) like the Vela pulsar (B0833−45), Geminga (J0630+17), B0656+14, and B1055−52, radiate thermal X-rays from the neutron star surface, possibly mixed with harder, nonthermal X-rays from the magnetosphere or a heated polar cap. The oldest objects that show X-ray emission, e.g., B0950+08 and B1929+10, radiate from their hot polar caps but are visible only because they are relatively nearby, within approximately 100 pc.

2. Accretion-driven X-ray emission could alternate with rotation-driven radio pulsations, in a mutually exclusive fashion, owing to intermittent or systematic switching between the two mechanisms. In unstable accretion flows, switching between accretion-driven and rotation-driven modes may occur sporadically. More systematic transitions may occur in binaries with large eccentricity, where accretion dominates at periastron while magnetospheric radiation occurs at apastron. The pulsar B1259−63 (Johnston et al. 1992), with an eccentricity of 0.8, may be a prototype of this class of object.

3. X-rays from ablated winds in objects like the eclipsing millisecond pulsar 1957+20 (Fruchter et al. 1992).

4. X-rays from interstellar gas shocked in pulsar wind nebulae, especially for high-velocity pulsars. These objects include the pulsars B1957+20 (Kulkarni et al. 1992; Fruchter et al. 1992), B1951+32 (Hester & Kulkarni 1988; Kulkarni & Hester 1988), B1929+10 (Wang, Li, & Begelman 1993), and J0437−4715 (Becker & Trümper 1993), The "Guitar Nebula" pulsar B2224+65 (Cordes, Romani, & Lundgren 1993) is also a good candidate for X-ray emission by such a process.

Motivated by these scenarios for X-ray emission associated with radio pulsars, we constructed a list of X-ray selected targets by analyzing images from the *Einstein* IPC, rejecting sources already identified, and then conducted a search at the

Arecibo Observatory for radio pulsations from the remaining targets. We also repeated measurements toward many sky positions as a countermeasure against interstellar scintillations. As a result of searching nearly 27 deg^2 of sky, we detected three new radio pulsars (J0631+10, J1843+20, and J1908+0457) and four others previously known (B0950+08, B1625+14, B1905+04, and B1929+10).

We discuss in § 2 our analysis of the X-ray images and other aspects of our selection of X-ray targets used in the radio pulsar search, which is described in § 3. The discovery of the young pulsar J0631+10, its association with the X-ray target, and a possible γ-ray detection from the EGRET instrument on board the *Compton Gamma-Ray Observatory* (*CGRO*) are included in § 4. The two other pulsars found in our search, J1843+20 and J1908+0457, are presented in § 5. In § 6 we discussed briefly the possibility of detecting the supernova remnant associated with J0631+10 and how many other such pulsars may have gone undetected in previous X-ray searches because of the higher absorption in the Galactic plane.

2. SELECTION OF X-RAY TARGETS

Early radio pulsar searches were confined to the Galactic disk (because that is where most pulsars are expected to be formed), resulting in the bulk of the pulsars known today. More recently, it has been recognized that a population of nearby millisecond pulsars would be nearly isotropically distributed on the sky, and untargeted searches have thus been carried out over hundreds of square degrees (Camilo 1994 and references therein). These searches have been highly successful in discovering fast pulsars, i.e., with periods below 100 ms (Phinney & Kulkarni 1994), but on the other hand, they can take several days of observing, especially if performed at high frequencies using large telescopes. At the Arecibo Observatory such searches are often done in "drift" mode, where the telescope is kept at a given azimuth and zenith angle, scanning the sky in strips of constant declination and with the integration time constrained by the time it takes for an object to cross the telescope beam. Recent Arecibo surveys (performed at sensitivities 1.7–2.5 times lower than ours) resulted in pulsar densities from around one per 40 deg^2 (Foster, Wolszczan, & Cadwell 1994) at high Galactic latitudes ($b > 20°$) to about one per 4 deg^2 near Galactic center (Nice 1994). Towards the Galactic anticenter, the pulsar density is about one per 10 deg^2. In choosing a targeted search of X-ray sources we were able to increase the integration time and the efficiency in detecting new interesting pulsars.

The most comprehensive survey of X-ray sources to date is the *Einstein Observatory* Catalog of IPC X-Ray Sources (or EOSCAT, Harris et al. 1990). Many of the EOSCAT sources have been identified with otherwise known astronomical objects, and thus, in order to enlarge our sample of targets (unidentified X-ray sources) for a radio pulsar search, we devised a new method of source detection (Zepka, Cordes, & Wasserman 1994) that allowed us to reliably detect new, fainter sources in the *Einstein* data. We applied our method to the 3445 IPC images available on CD-ROM (Harris et al. 1990) for which an estimate of the background noise was available. A complete list of the X-ray sources discovered by our method and the comparison with previous X-ray surveys will be published elsewhere. As an example, we show in Figure 1*a* the IPC image (field number I7237) that contains the X-ray source that may be associated with pulsar J0631+10.

Our method compares the histogram of counts from the entire image with that expected for noise only. A test is applied to each histogram bin to determine the probability that the number of counts is within the range expected from statistical fluctuations in the background. If this probability is below a given present threshold, all corresponding pixels in that bin are selected (see Figs. 1*c*–1*d*). Finally the selected pixels from all bins that pass this test are divided into groups of neighboring pixels, each group being a "detected source" (denoted by circles in Fig. 1*b*).

By applying the histogram method to the IPC images, we obtained a list of 6783 X-ray sources, 3638 of which were in common with sources in the EOSCAT catalog, accounting for approximately 80% of all EOSCAT sources detected in those fields. All EOSCAT sources for which an identification was provided (1451 in total) were excluded from our list of radio targets. In addition, we cross correlated our source coordinates with several other catalogs (of galaxies, white dwarfs, pulsars) to arrive at a final list of 4704 target sources. Finally, we selected 1900 in the range of observable declinations of the 305 m Arecibo radio telescope to perform a search for radio pulsars.

3. RADIO SEARCH

To date, nearly 1300 of the selected targets have been observed at 430 MHz. About one-third of these have been reobserved at least once as a countermeasure against interstellar scintillation. Each beam position was integrated for 3.1 minutes with a sample time of 180 μs, corresponding to 2^{20} time samples. The data-taking hardware included a filter bank that divides the 8 MHz bandpass into 32 channels of 0.25 MHz bandwidth, resulting in 32 time series digitized to 3 bits per sample. The off-line data processing consisted of the following basic steps: (1) undo the dispersive delays in frequency caused by propagation through the ionized interstellar medium; (2) apply a fast Fourier transform (FFT) to obtain the frequency power spectrum; (3) sum harmonics of a candidate pulsar frequency (to a maximum of eight per trial) to maximize signal-to-noise ratio (S/N); (4) remove redundant pulsar candidates from different trial dispersion measures (DMs); and (5) remove any known radio frequency interference (RFI). This last step is essential to reduce the number of pulsar candidates to a manageable number (meaning, a few per beam), as RFI at the Arecibo Observatory can easily overwhelm the signal of a faint pulsar.

Since the 430 MHz radio beam at Arecibo has a radius of about 5′, the total sky area coverage in the survey was about 27 deg^2. Taking into account the different integration time used in Arecibo untargeted searches and the density of discovered pulsars, we estimate one new pulsar should be detected serendipitously for each 30 deg^2 of high Galactic latitude sky covered by our search, while near the Galactic plane ($|b| \leq 5°$) the pulsar density should be close to one per 2 deg^2. We have so far discovered three new pulsars (PSR J0631+10, J1843+20, and J1908+0457) and rediscovered four others previously known: B0950+08, PSR 1625+14, PSR B1905+04, and B1929+10. Two of them (B0950+08 and B1929+10) are known X-ray emitters and were found only because their strong radio emission was detected in the telescope sidelobes. The other two are clearly chance discoveries since they are at least 4′ away from their respective X-ray sources. Of the pulsars found, B1625+14 and B0950+08 are located at high Galactic latitude ($b > 20°$); all others, with the exception of J1843+20 ($b = 11°$), are in the Galactic plane ($|b| < 5°$). A more extensive description of this search and its significance for pulsar population models will be published elsewhere.

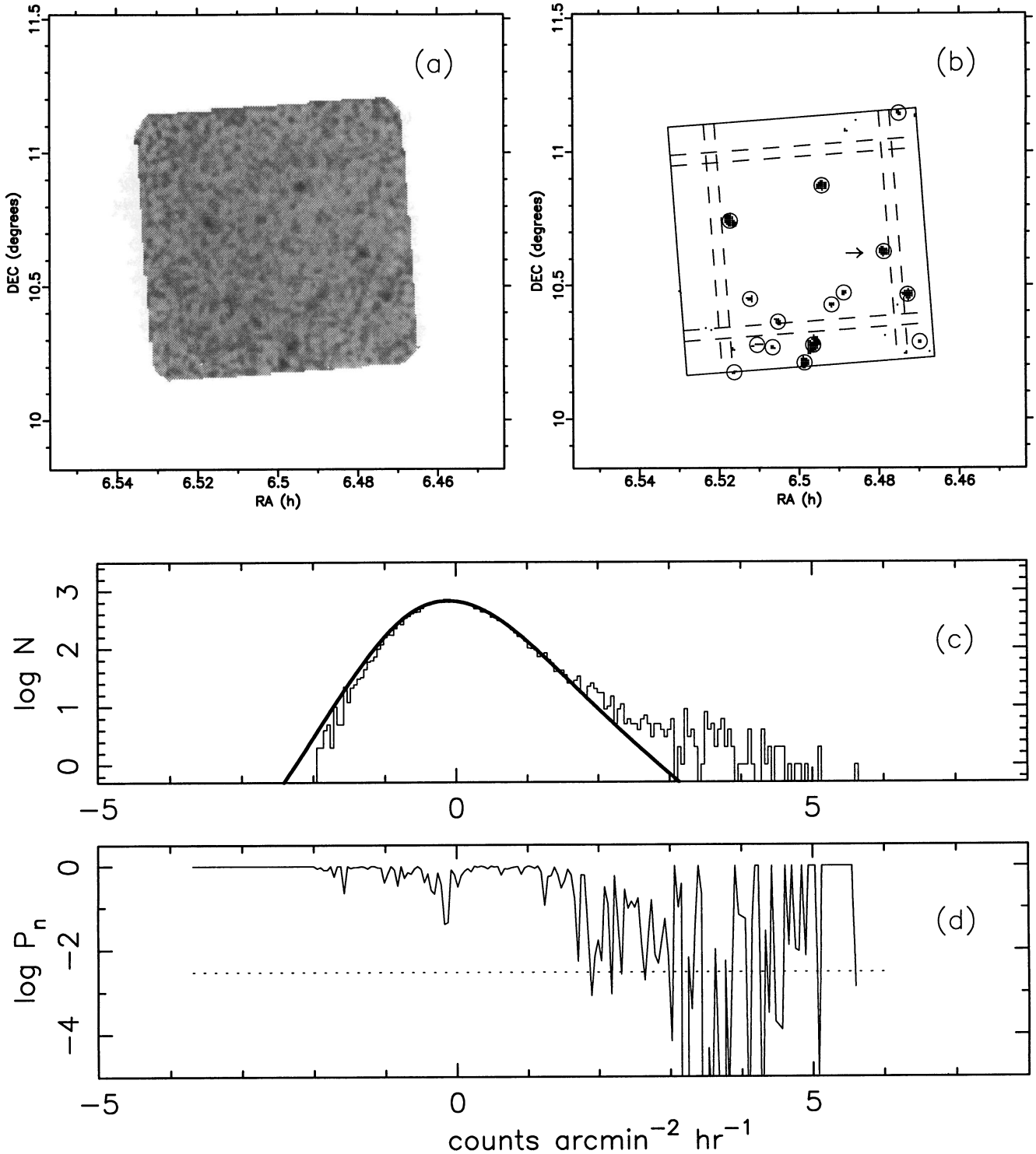

FIG. 1.—(*a*) *Einstein* IPC image containing pulsar J0631 + 10; (*b*) sources detected in this IPC image (denoted by circles). An arrow indicates the X-ray source 2E 1676. Dashed lines correspond to regions of lower sensitivity due to shadowing from the IPC detector supporting ribs. (*c*) Histogram of counts from the image in (*a*) with calculated background histogram superposed (*thick solid line*). (*d*) The probability P_n that the number of counts in a given histogram bin n is larger than what is expected from noise only, and thus potentially due to sources contained in the image. The threshold $\bar{P} = 0.003$ in shown as a dotted line.

4. THE INTERMEDIATE-AGE PULSAR, PSR J0631+10

In this section we describe the results from radio, X-ray, and γ-ray observations of J0631+10. In addition to presenting the observed and derived parameters, we discuss the possibility of an association between the X-ray source and radio pulsar.

4.1. *Radio Observations*

Timing measurements on J0631+10 have been performed since the confirmation of its discovery in 1993 May, using the XCORHI timing data acquisition system at the Arecibo Observatory. Pulse times of arrival (TOAs) were obtained for 1 minute averages at 1400 MHz and higher frequencies, while usually 3 minutes were needed at 430 MHz to produce large enough S/N to obtain TOAs. The best timing model was fitted using the TEMPO package (Taylor & Weisberg 1989). Observed and derived radio parameters are given in Table 1, with the timing residuals plotted in Figure 2. The pulsar's young age and large period derivative would suggest that timing noise and glitches might be present. In contrast, the timing model fits the TOAs fairly well (especially at high frequencies, where the pulse is sharp and relatively strong). Although long-term timing noise ($\tau_{noise} > 1$ yr) cannot be ruled out, no short-term variability or glitches have been detected.

The average pulse profile at 1400 MHz and higher frequencies is unusually narrow and symmetric (Figs. 3*b*–3*d*), dominated by two very sharp peaks (width per peak less than 3°, while the separation between peaks is ~5°) with near-zero emission at the center, and at least two additional components on each side, suggesting a double cone of emission. At 430 MHz (Fig. 3*a*) the pulse is broader, with the double peak unresolved.

There is no clear indication of an asymmetric scattering tail in the profile. Nevertheless, suspecting that the broader 430

TABLE 1

PSR J0631+10 OBSERVED AND DERIVED RADIO TIMING PARAMETERS

Parameter	Value
α (J2000)	$06^h31^m27^s.6 \pm 0^s.1$
δ (J2000)	$+10°36'58'' \pm 2''$
Galactic longitude, l	201°.2
Galactic latitude, b	0°.45
Period, P	0.28774974800(3) s
Period derivative, $\dot{P}$	$104.626(1) \times 10^{-15}$
Epoch of period (MJD)	49133.5
Dispersion measure, DM	125.64(1) pc cm^{-3}
Mean flux density at 430 MHz, S_{430}	1.5 mJy
Mean flux density at 1400 MHz, S_{1400}	0.8 mJy
Distance from TC93 model	6.5 kpc
Assumed distance	1.0 kpc
Spin-down luminosity, $\dot{E} = I\Omega\dot{\Omega}$	5.4×10^{34} ergs s^{-1}
Magnetic field strength, B	5.7×10^{12} G
Spin-down age, $\tau = P/(2\dot{P})$	43,000 yr

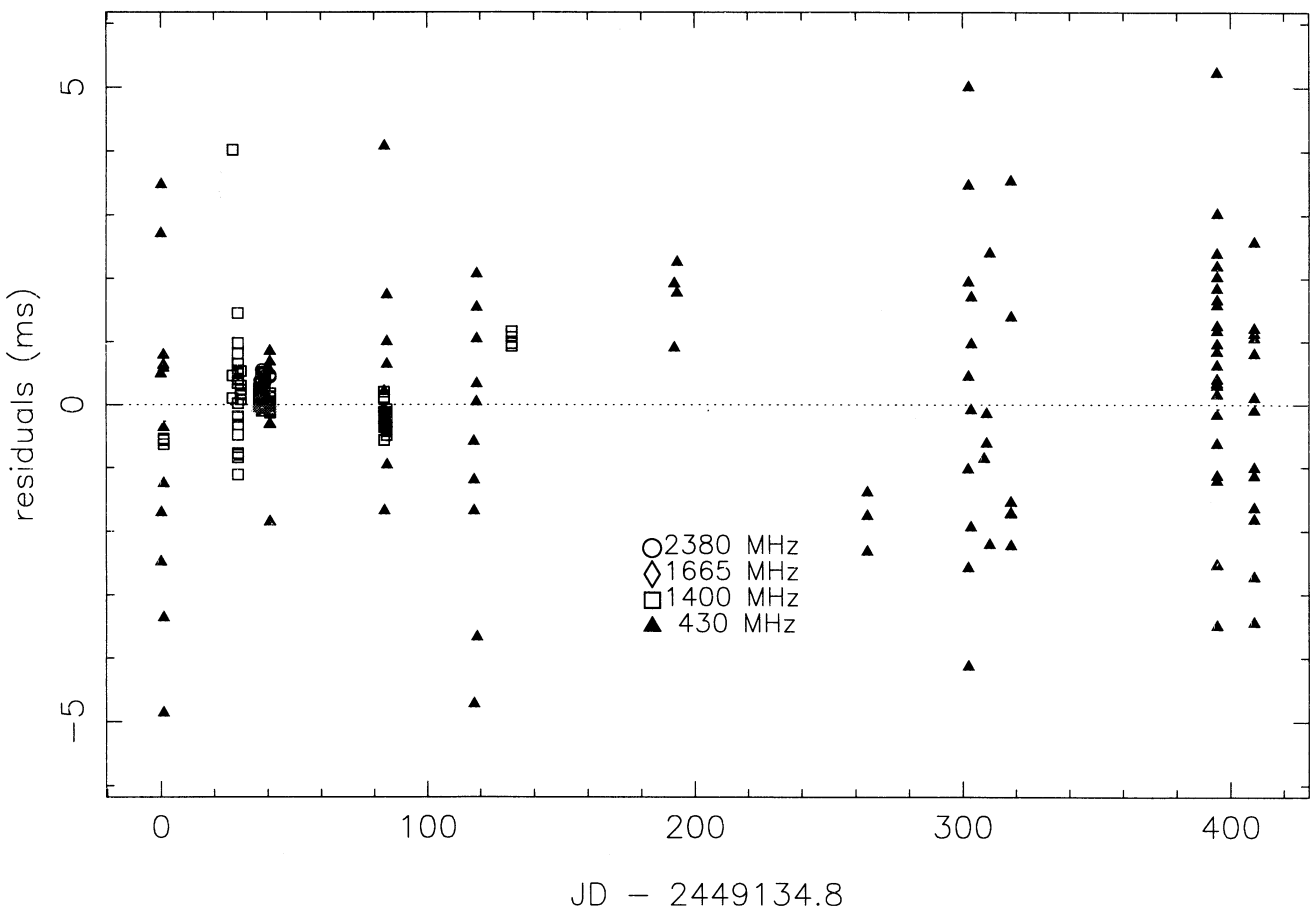

FIG. 2.—Timing residuals for J0631+10 at various frequencies from the model shown in Table 1

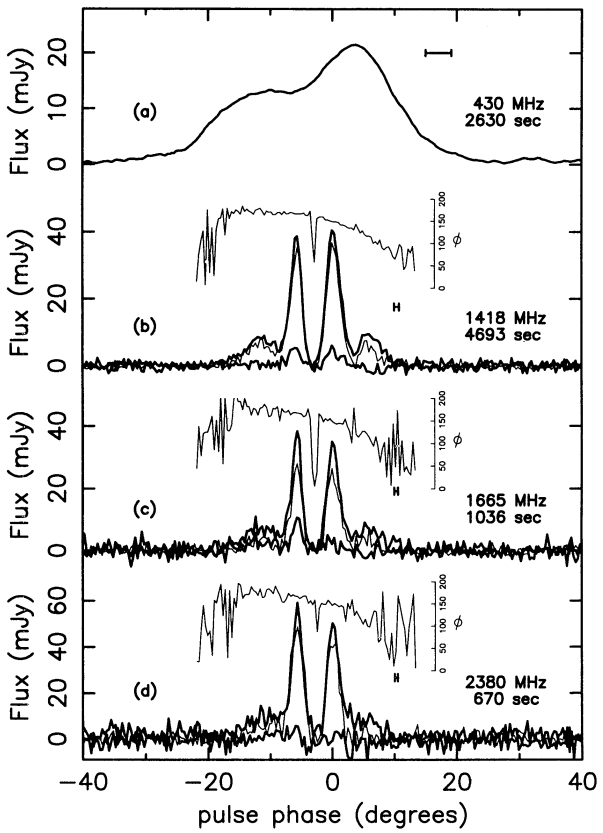

FIG. 3.—Average pulse profile at several frequencies: (*a*) 430 MHz, (*b*) 1400 MHz, (*c*) 1665 MHz, and (*d*) 2380 MHz. The total integration time is shown below each frequency. With the exception of 430 MHz, the pulsar shows a high degree of polarization indicated as thin (linear polarization) and thick (circular polarization) lines below each corresponding pulse profile. The polarization position angle ϕ is plotted above the intensity profiles at the three highest frequencies. At some point between the central peaks, the absence of emission makes ϕ assume some random value. A horizontal bar to the right of each profile indicates the effective time resolution.

MHz pulse profile is at least in part due to scattering, we convolved the 1400 MHz profile with the one-sided exponential $e^{-\theta/\theta_{sc}}$ (where θ is pulse phase and θ_{sc} is the broadening due to scattering) and smoothed the profile with a box function with the same width as the time resolution at 430 MHz (3.2 ms). We find that $\theta_{sc} \sim 6°$ (corresponding to a timescale of $\tau = 5$ ms) can account for much of the broadening without producing a noticeable exponential tail. On the other hand, such a value of τ is too small to reproduce the full width of the 430 MHz pulse profile, suggesting that an intrinsic change in the pulse shape is also present. As a matter of comparison, we calculated the expected scattering timescale from the parabolic fit of τ as a function of the dispersion measure of known pulsars obtained by Cordes, Spangler, & Weisberg (1994). Rescaling their result to 430 MHz ($\tau \propto \nu^{-4.4}$), we estimate that for J0631+10 (DM = 125 pc cm^{-3}) the scattering timescale is contained in the interval $0.2 < \tau(\text{ms}) < 8$, which makes our previous estimation of $\tau \sim 5$ ms a plausible one.

The pulsar was easily detected up to 2380 MHz (the maximum available frequency at the time of the observations) with a nearly flat spectral index ($\alpha \sim 0$, $S_\nu \propto \nu^\alpha$) down to 1400 MHz. From 1400 to 430 MHz the spectral index is steeper with $\alpha \sim -0.6$. On the other hand, because of the narrower pulse, when integrating over the region of the profile where there is emission, the flux is higher at 1400 MHz (9 mJy) than at 430 MHz (7 mJy).

We observed high degrees of linear polarization for J0631+10 at the higher frequencies, reaching over 80% at 1400 MHz. The swing of the position angle can be easily seen (above the pulse profiles in Figs. 3*b*–3*d*), though it does not present the usual S shape (Blaskiewicz, Cordes, & Wasserman 1991). On the other hand, the pulsar shows little polarization (<10%) at 430 MHz. To explain this fact as the result of Faraday depolarization, the rotation measure (RM = 0.81 rad m^{-2} $\int dl\, n_e B_\parallel$) must be large enough to make the position angle ϕ of the polarization vector rotate by at least π radians within the 5 MHz bandwidth used in the timing measurements. Since $\phi = c^2 \text{RM}/\nu^2$, this requirement implies that RM $\sim$ 300 rad m^{-2}. In addition, the ratio RM/DM provides a direct measurement of the mean interstellar magnetic field along the line of sight, or (e.g., Manchester & Taylor 1977) $\langle B_\parallel \rangle$ = RM/0.81 DM ~ 3 μG, which is a reasonable value for the Galactic anticenter (Manchester 1974).

According to a model of the Galactic electron density (Taylor & Cordes 1993, hereafter TC93), a DM of 125.3 pc cm^{-3} corresponds to a distance of about 6.5 kpc. This large value (the highest among all known pulsars in the Galactic anticenter) actually gives an upper limit for the distance since the TC93 model does not take into account local inhomogeneities. The dark cloud LDN 1605 (Lynds 1962) and ionized material associated with the star-forming region 3 Mon in the pulsar's foreground are likely to be responsible for much of the dispersion (see § 4.3). Such a large mismatch of the predicted and actual distances has been observed before: Frail, Kulkarni, & Vasisht (1993) suggest that pulsar B1758−23 is probably associated with supernova remnant W28, which lies about 3 kpc away, even though its predicted distance by the TC93 model is 13.8 kpc. The authors attribute nearly 90% of its dispersion measure (1063 pc cm^{-3}, the highest of any known pulsar) to a dense screen of ionized material (possibly associated to H II regions) along the line of sight.

In the remainder of this paper we assume J0631+10 to be at 1 kpc, which is also consistent with the amount of X-ray absorption expected (§ 4.4) and the efficiency of γ-ray emission for the pulsar (§ 4.6).

4.2. *X-Ray Source and Radio Pulsar Positions*

Our analysis of the I7237 IPC image of the dark cloud LDN 1605 redetected the EOSCAT source 2E 1676, which has a count rate of 0.0075 ± 0.0013 counts s^{-1}, corresponding to S/N = 5.6 σ in this 12 ks exposure. Its <50 net counts are insufficient to allow a search for pulsations, in part because our current radio timing model for J0631+10 cannot be reliably extrapolated back to the epoch of *Einstein* observations, over 10 years ago.

The X-ray coordinates ($\alpha = 06^h31^m28^s.8$, $\delta = +10°35'45''$) have a published uncertainty of 51″ in the EOSCAT, but the actual error is probably larger because the source is partially shadowed by one of the structure "ribs" that support the IPC detector. Unfortunately, it is difficult to quantify the exact effect of shadowing on the point-spread function (PSF), count rate, and spectrum of the source since it will depend strongly on where in the rib's shadow the source is located, how much of the source has been covered, and the spectrum of the X-ray source. Our radio timing measurements of the pulsar have yielded a position at $\alpha = 06^h31^m27^s.6$, $\delta = +10°36'58''$, with an accuracy better than 10″. The corresponding separation of

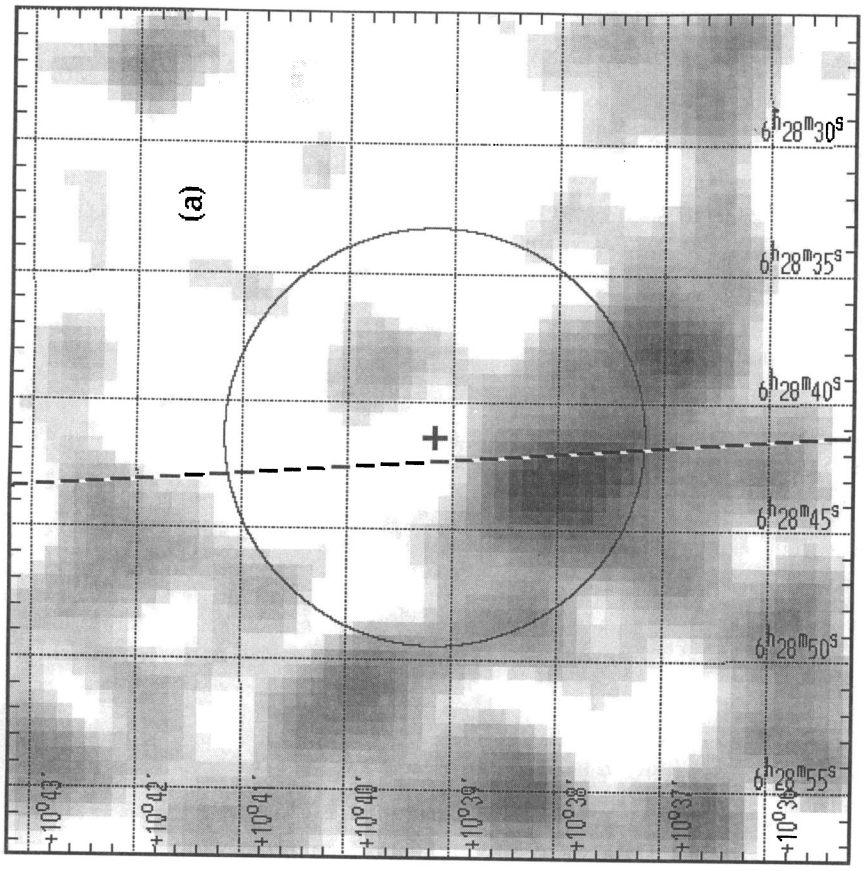

FIG. 4a

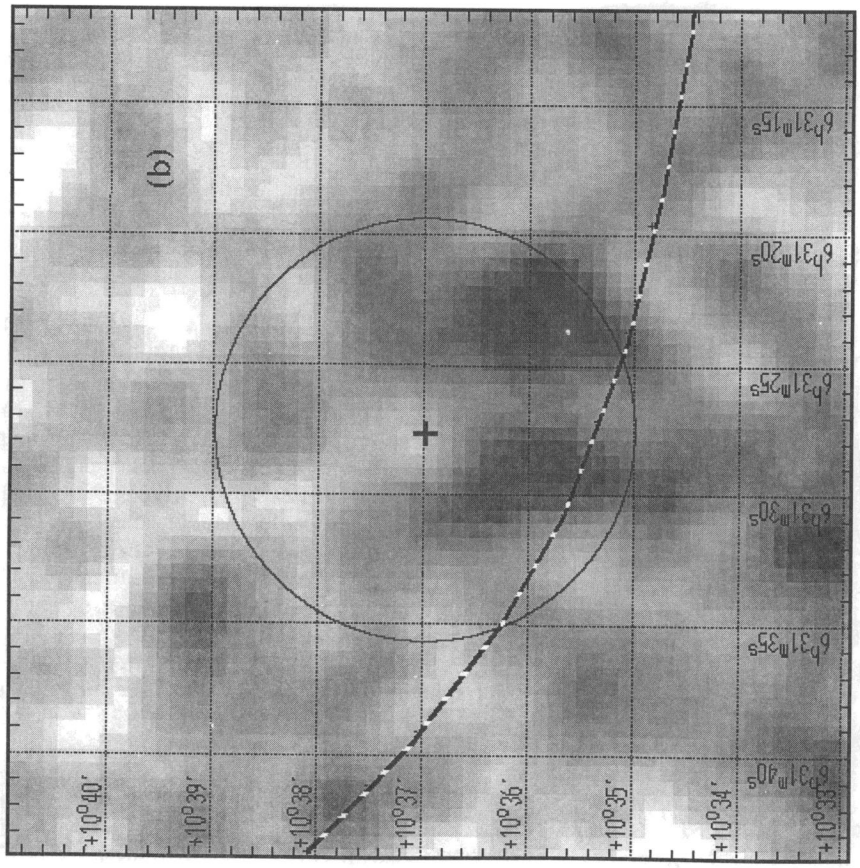

FIG. 4b

FIG. 4.—(*a*) Blowup of *Einstein* IPC field I7237 containing PSR J0631 + 10. The 2′ circle radius corresponds approximately to the positional uncertainty for an X-ray source located at the radio pulsar position (indicated by the cross). The centroid of the source 2E 1676 lies approximately 75″ to the south of the cross. B1950 coordinates apply. The field of view is 8′ × 8′ and each pixel measures 8″. The region to the right of the dashed line lies under the shadow of the supporting rib in the *Einstein* IPC. (*b*) Blowup of *ROSAT* PSPC image containing J0631 + 10. Same scale and conventions apply as in (*a*), except that the coordinates are now J2000. The region above the dashed line corresponds to the PSPC central rib shadow.

$\sim 75''$ is still consistent with an association between pulsar and X-ray source, since the radio position is well inside the rib shadow where the sensitivity is further reduced by 50% or more (Harris et al. 1990; D. Harris, personal communication). The *Einstein* source and error boxes and their relative position to the rib shadow are shown in Figure 4*a*. Based on the density of known pulsars at the Galactic anticenter (~ 1 deg^{-2}) and the amount of sky covered in our pulsar search (fewer than 200 anticenter sources surveyed), the probability of a chance pulsar discovery within 75″ of a surveyed anticenter X-ray source is less than 1%.

In addition to the *Einstein* exposure, we have obtained a *ROSAT* image (Fig. 4*b*) containing J0631+10 from two independent PSPC exposures of MON OB1 totaling 10 ks (D. Burrows, personal communication). A *ROSAT* counterpart of 2E1676 was detected in *both* exposures. Unfortunately, this source is also shadowed by the detector supporting ribs, increasing the uncertainties in position, flux, and spectrum, as for the *Einstein* IPC observations. The PSPC detector has an additional complication: its PSF degrades substantially with off-axis angle (Hansinger et al. 1993), reaching about 1′ at the pulsar position (25′ from the image center). For this reason, the separation of 60″ is consistent with this PSPC source being associated with J0631+10. The source looks extended with two cores, but because of the number of counts and rib shadowing, it is unclear whether that is an artifact or evidence of nebular emission near the pulsar.

Since the thermal X-ray emission expected from intermediate-age neutron stars peaks below 1 keV, the *ROSAT* PSPC has been very efficient in detecting thermal X-rays at higher count rates than the *Einstein* IPC. A 2′ radius detection cell centered on the pulsar's position yields a PSPC background-subtracted count rate of about 0.005 counts s^{-1} (0.1–2.5 keV). The surprisingly low PSPC flux for this exposure of J0631+10 is due in part to shadowing, but interstellar absorption (mostly of soft X-ray photons) by the dark cloud LDN 1605 in the foreground (see § 4.3) could also play a major role in decreasing the X-ray flux of J0631+10 as well. An intrinsically harder spectrum would also produce a higher IPC count rate, but a hard spectrum is unlikely in light of observations of other X-ray–emitting pulsars of similar age (e.g., B1055−52, B0656+14 and Geminga), which show an X-ray spectrum dominated by the soft (assumed thermal) component ($kT < 0.1$ keV).

4.3. *The Dark Cloud LDN 1605*

PSR J0631+10 was discovered by targeting an unidentified source detected in an IPC exposure of the dark cloud LDN 1605. This cloud is part of the large and active star-forming region 3 Mon, which is composed of reflection nebulae (S Mon), H II regions (IC 446–447, IC 2167–69), young star clusters (NGC 2245–2247, Mon OB1) and dark clouds (LND 1604–1610).

Shevchenko & Yabukov (1988) estimate 3 Mon's mass to be $5 \times 10^4\ M_\odot$ and its distance to be approximately 0.75 kpc, with a projected size of 10 × 50 pc. Assuming its radial extent to be 10 pc, we obtain a mean hydrogen density of 400 cm^{-3}. This value is likely to be higher toward the position of J0631+10, which is near one of the two cores of 3 Mon. The corresponding hydrogen column density of approximately 10^{22} cm^{-2} will absorb most of the X-rays up to about 0.75 keV.

With the exception of the Gum Nebula, the TC93 model for the electron density distribution in the Galaxy does not explicitly account for local enhancements of the electron density due to, for example, H II regions. Without correcting for these, the model puts J0631+10 at a distance of 6.5 kpc. With 1605 at a distance of 0.75 kpc, the pulsar is either in or behind the cloud; therefore, it is possible that its high DM is due in large part to ionized material associated with the cloud. For a column density of 10^{22} cm^{-2}, an ionization fraction of 3% would account for an increase of 100 pc cm^{-3} in the observed DM. Such a value is at least two orders of magnitude above the typical ionization fraction of dark clouds from cosmic rays and carbon ionization (Kulkarni & Heiles 1988). On the other hand, many H II regions are associated with 3 Mon, and if one or more intersect the line of sight to J0631+10, their contribution could be enough (Weisberg 1978) to put the pulsar just beyond 3 Mon, at a distance of approximately 1 kpc, or even inside it. This last possibility is particularly interesting since there could be observable emission from the interaction of the pulsar's magnetosphere and the dense cloud medium.

4.4. *Energetics*

The spin-down energy of J0631+10 ($\dot{E} = -I\Omega\dot{\Omega} \sim 5.4 \times 10^{34}$ ergs s^{-1}, assuming $I = 10^{45}$ g cm^{-2} here and in the remainder of this paper) is larger than those of B0656+14, B1055−52, and Geminga (all X-ray emitting isolated neutron stars) by factors of 1.4, 1.8, and 1.6, respectively. Since there is a positive correlation between $\dot{E}$ and X-ray luminosity for previously known X-ray–emitting pulsars (Ögelman 1994), J0631+10 is a likely candidate for X-ray emission. The main issue in this section is whether the observed X-ray counts are consistent with the anticipated X-ray luminosity and the estimated distance.

Making use of the PROS data analysis package, we obtained a crude spectrum for the IPC source 2E 1676 shown in Figure 5*a* together with its best blackbody fit ($kT = 0.27 \pm 0.08$ keV and $N_{\rm H} = 9 \pm 4 \times 10^{21}$ cm^{-2}). The large uncertainty in the fitted parameters is due to the small number of counts from the source. The resulting observed X-ray flux and luminosity are, respectively, $F_{\rm X} = 1.9 \times 10^{-13}$ ergs cm^{-2} s^{-1} (4.4×10^{-12} ergs cm^{-2} s^{-1} unabsorbed) and $L_{\rm X} \sim 1.3 \times 10^{32} d_{\rm kpc}^2$ ergs s^{-1} (where $d_{\rm kpc}$ is the distance in kpc). All values of X-ray luminosity quoted in this paper are within the corresponding instrument energy band (0.16–3.5 keV for *Einstein* IPC; 0.1–1.5 keV for *ROSAT* PSPC) and assume emission over 4π sr. In addition, the spectral analysis does not take into account the unknown effect of rib shadowing, and thus the results shown here are approximate.

In order to assess the quality of the blackbody fit to the data, we calculated χ^2 contours for the fitted parameters T and $N_{\rm H}$ (*solid curves* in Fig. 5*b*). Although the large uncertainties allow a wide range of possible fits, it is unlikely that the column density is much above 10^{22} cm^{-2}. A model for the distribution of the mean column density integrated across the Galaxy gives $\langle N_{\rm H} \rangle \sim 5 \times 10^{21}$ cm^{-2} (Harris et al. 1990) in the direction of J0631+10, and although an increase by a factor of 2 is likely, a factor of 10 is probably unrealistic. Also, no other X-ray–emitting pulsar with age similar to J0631+10 has a blackbody component with a temperature above 0.3 keV (Ögelman 1994). Our best blackbody fit (*cross* in Fig. 5*b*) is consistent with both of the above empirical statements.

In addition, we include in Figure 5*b* dashed contours corresponding to different "effective radii" of the X-ray–emitting region, $r_{\rm eff} = (A/4\pi)^{1/4}$, where $A = L_{\rm X}/F_{\rm X}$ and $F_{\rm X}$ is the *unab-*

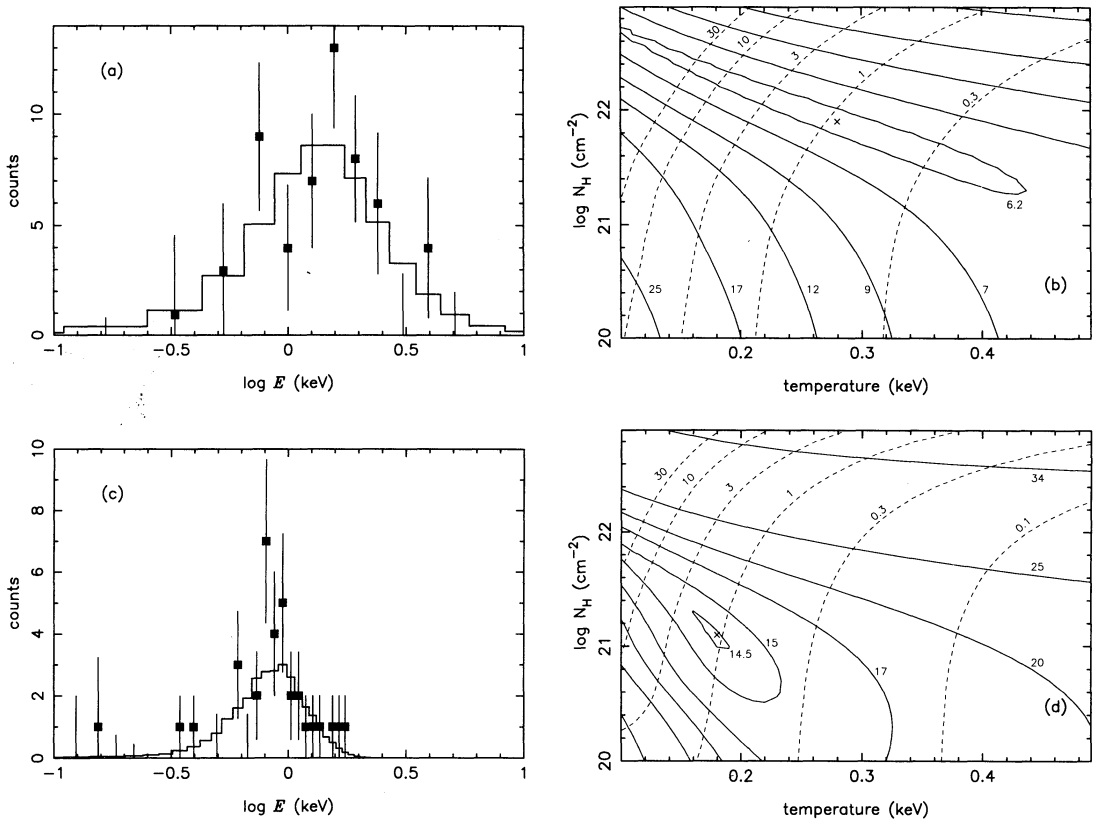

FIG. 5.—(*a*) IPC spectrum of 2E 1676 (*data points*) with blackbody fit superposed (*histogram*), where $kT = 0.27$ keV and $N_H = 9.1 \times 10^{21}$ cm^{-2}. (*b*) Contours of χ^2 for a blackbody fit to the IPC data. Numbers next to the solid line contours are the values of χ^2. The dashed lines correspond to different values (in kilometers) of $r_{eff} = (A/4\pi)^{1/2}$, where $A = L_X/4\pi F_X$ is the are of the emitting region. (*c*) X-ray spectrum of the *ROSAT* PSPC source at the location of J0631+10. The histogram shows the best fit for an absorbed blackbody ($N_H = 1.2 \times 10^{21}$ cm^{-2} and $kT = 0.18$ keV). (*d*) The corresponding χ^2 contours and sizes of the emitting region for the *ROSAT* source, as in (*b*).

sorbed X-ray flux at the star's surface. Note that since $A = \Omega r^2$ for emission from a solid angle Ω on the surface of a sphere of radius r, then $r_{eff}/r = (\Omega/4\pi)^{1/2}$. The best fit in Figure 5*b* implies $r_{eff} \sim 1$ km (or $\Omega \sim 0.1$ sr, for $r = 10$ km). In comparison, the expected area of a pulsar polar cap is $A_{PC} \sim 0.07P^{-1}$ km^2 (P is the period in seconds), which translates into an effective radius $R_{PC} = (A_{PC}/4\pi)^{1/2} \sim 0.3$ km for J0631+10.

We applied a similar analysis to the *ROSAT* exposures of this region, after combining them into a single 10 ks exposure. The data and best blackbody fit ($kT = 0.18 \pm 0.08$ keV, $N_H = 1.2 \pm 0.6 \times 10^{21}$ cm^{-2}) are shown in Figure 5*c*. The effective radius of the emitting region for the best *ROSAT* blackbody fit (*dashed contours* in Fig. 5*d*) is approximately 1 km. The χ^2 contours for *ROSAT* (Fig. 5*d*) and *Einstein* sources (Fig. 5*b*) have very different minima, but they are compatible given the large uncertainties in the fitted parameters.

For the *Einstein* data, we find that a power-law model ($f_X \propto E^{-\alpha}$, where f_X is the X-ray energy flux density) with energy index $\alpha = 4 \pm 3$ and $N_H = 1.4 \pm 0.3 \times 10^{22}$ cm^{-2} fits the data equally well, corresponding to $L_X \sim 2.3 \times 10^{34} d_{kpc}^2$ ergs s^{-1}. This value would imply an X-ray emission efficiency near 50%, which is at least 10 times larger than the efficiency of any known X-ray–emitting pulsar. Still, we cannot discard the possibility of a power-law spectrum because of the large uncertainty in α. In both the power-law and the blackbody fits, the value of N_H is rather well constrained around $\lesssim 10^{22}$ cm^{-2} and is in agreement with the value that we estimate for the contribution of LDN 1605 in § 4.3. In Figure 6 we show the contours of χ^2 (*solid lines*) and of constant $L_X/\dot{E}$ for the power-law fit.

Our measured values of the IPC X-ray luminosities for J0631+10 are consistent with those of pulsars of the same age if located 1 kpc away and, more importantly, with its measured spin-down energy ($\dot{E} \sim 5.4 \times 10^{34}$ ergs s^{-1}). Because of the small number of X-ray counts and of shadowing effects in both *Einstein* and *ROSAT* exposures, the results presented in this paper on the nature of the X-ray emission from J0631+10 are still inconclusive. A deep exposure with the *ASCA* (*Astro-D*) satellite would help clarify the situation.

4.5. *Search for γ-Ray Emission*

Seven rotation-driven neutron stars have been detected as γ-ray pulsars: B0531+21, B0540−69, B0630+17, B0833−45, B1055−52, B1509−58, and B1706−44. Since J0631+10 is younger and has a higher $\dot{E}$ than Geminga (B0630+17) and B1055−52, it is quite possible that J0631+10 is a γ-ray emitter as well. Here, we discuss this possibility by utilizing data from the EGRET detector aboard the *CGRO* γ-ray telescope.

The EGRET detector has a large field of view ($\sim$0.6 sr), so that previous observations of the Crab and Geminga pulsars also contained J0631+10. We took advantage of this fact to use publicly available data to search for modulations at the radio period of J0631+10. If no glitches have happened since the EGRET observations, we expect our timing model to be

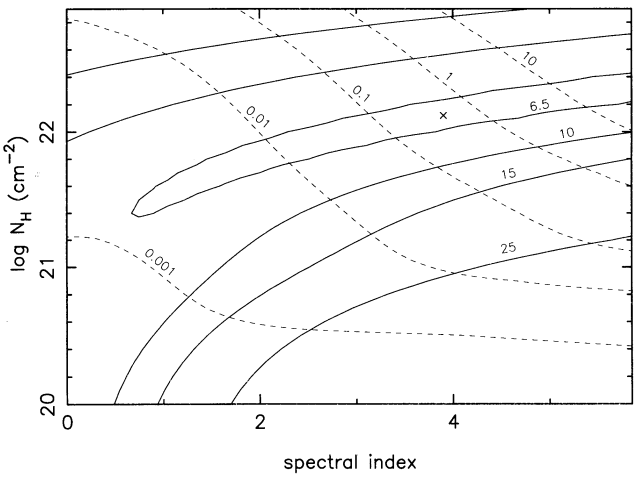

FIG. 6.—Contours of constant χ^2 (*solid*) and X-ray luminosity L_X (*dashed lines*) as obtained by fitting a power-law to the *Einstein* data. The values of L_X are normalized to the measured spin-down luminosity $\dot{E} = 5.4 \times 10^{34}$ ergs s^{-1}.

able to predict the period accurately enough to detect γ-tray modulations if they are indeed present at high pulse fractions.

In Figure 7 we show the result of folding EGRET data taken in 1991 May (viewing period 1 of GRO), during the pointing toward the Crab pulsar. We applied several statistical tests to evaluate the significance of the modulations observed. A low-energy cutoff of 170 MeV and an energy-dependent cone of acceptance $\theta = 5.85(E_\gamma/100\ \mathrm{MeV})^{-0.534}$ degrees (J. Fierro, private communication) yielded a H-test value of 14 (De Jager et al. 1989), which is consistent with the modulations having only 0.4% chance of being randomly generated. Although this result is tantalizing, it is certainly not conclusive, since a small change in the energy cutoff can increase this probability substantially. On the other hand, repeating this procedure for a grid of 5 × 5 beams separated by 10° centered on J0631+10 while keeping the folding parameters unchanged gives results consistent with noise. All grid points (with the exception of three that contain counts from Geminga) had fewer counts

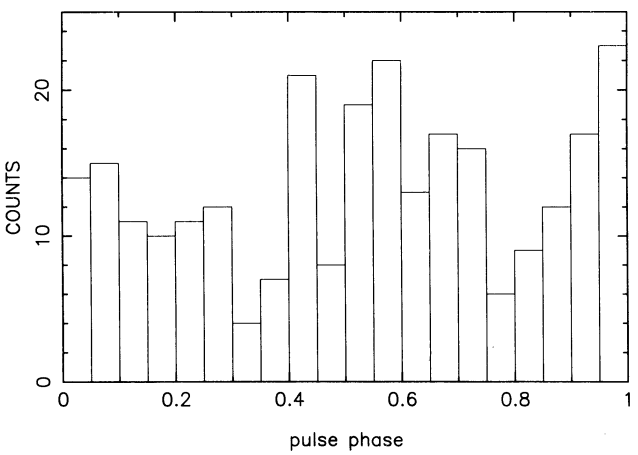

FIG. 7.—Profile obtained by folding EGRET γ-ray photons using the model in Table 1. The energy-dependent acceptance cone has a radius $\theta = 5.85$ $(E_\gamma/100\ \mathrm{MeV})^{-0.534}$ degrees, and only photons with energies above 170 MeV are included. A total of 267 counts is included in this histogram. The probability that such modulations can be generated by noise is less than 1%.

than the point centered on J0631+10. In addition, folding photons at the location of J0631+10 with Geminga's timing model does not yield pulsations, which assures that these photons are not due to spillover from Geminga.

At the location of J0631+10, we obtain a total of 267 counts with energy above 170 MeV (and using the energy-dependent cone of acceptance). Using the number of counts from nearby beams from the grid described above as a mean background, we estimate that approximately 150 net excess counts are coming from the beam centered on J0631+10. If we assume that these counts are generated by the pulsar with a mean energy of 250 MeV per photon, the resulting γ-ray flux is approximately 4.3×10^{-10} ergs cm^{-2} s^{-1}. Therefore in order to avoid 100% γ-ray efficiency we require its distance to be at the most 2.0 kpc $(2\pi/\Omega_\gamma)^{1/2}$ (where Ω_γ is the solid angle swept out by the γ-ray beam). If J0631+10 is actually 1 kpc away, this efficiency goes down to approximately 25%, which is comparable to the efficiencies estimated for Geminga and B1055−52.

5. J1843+20 AND J1908+0457

Two other pulsars, J1843+20 and J1908+0457, were discovered in our search. Their timing parameters are displayed in Table 2. PSR J1843+20 (Fig. 8*a*) is a 3.4 s pulsar 11° above the Galactic plane, with DM = 80 pc cm^{-3}, corresponding to a distance of approximately 6 kpc using the TC93 model. Timing measurements have not yet determined a value for $\dot{P}$. The estimated X-ray luminosity for the IPC source (assuming a blackbody model and a distance of 6 kpc) is $L_X \sim 3.0 \times 10^{32}$ ergs s^{-1}. Therefore, in order for the observed X-rays to be generated by the pulsar, the period derivative has to be greater than 10^{-11}, which is an order of magnitude larger than the highest $\dot{P}$ known. Observations at 1400 MHz put the distance between the center of the X-ray source and radio pulsar below 2′, but since the radio position is uncertain to about the same amount and the X-ray error box is about 1′.5, an association cannot be ruled out yet based on positional information only. The X-ray source detected by our method was not found by previous processings of the *Einstein* data and therefore is not included in the EOSCAT.

The other slow pulsar found, J1906+0457 (Fig. 8*b*), has a period of 0.85 s and DM = 360 pc cm^{-3}. This pulsar was found when targeting 2E 4186, a 6 σ X-ray source contained in an IPC exposure of the nearby supernova remnant W50. Because J1908+0457 is an old pulsar ($\tau \sim 10^7$ yr), it is clearly not associated with W50. Coincidentally, another pulsar was detected by the search algorithm in the same beam area that contains J1908+0457. This other pulsar, B1905+04, was found in a search by Fruchter (1989), but it was unknown to us at the time of our search. Because its dispersion measure (217 pc cm^{-3}) is significantly smaller than that of J1908+0457, we rule out the possibility that the two pulsars are members of a disrupted binary. The discovery of a pulsar in a part of the sky that has been previously searched using the same telescope is significant and may imply that many others have been missed, particularly those with large values of DM.

At the time of the discovery of J1908+0457, F. Camilo (Princeton) and D. Nice (NRAO) were carrying out timing observations of several pulsars, including B1905+04. They were able to reprocess their data to obtain the timing parameters and an accurate position for J1908+0457 in a relatively short time. The period derivative ($\dot{P} = 1.3 \times 10^{-15}$) and large DM (and consequently large distance) make it unlikely that

TABLE 2

PSR J1843+20 AND J1908+0457 OBSERVED AND DERIVED RADIO TIMING PARAMETERS

PARAMETER	VALUE	
	PSR J1843+20	PSR J1908+0457
α (J2000)	$18^h43^m58^s \pm 8^s$	$19^h08^m16^s.15 \pm 0^s.1$
δ (J2000)	$+20°26' \pm 2'$	$+04°57'41'' \pm 2''$
Galactic longitude, l	50°.5	39°.3
Galactic latitude, b	+10°.7	−1°.47
Period, P (s)	3.40657162 (5)	0.8467928462 (4)
Period derivative, $\dot{P}$	...	$0.98(3) \times 10^{-15}$
Epoch of period (MJD)	...	49079.5
Dispersion measure, DM (pc cm^{-3})	80	360
Distance from TC93 model (kpc)	6.0	9.3
Spin-down luminosity, $\dot{E} = -I\Omega\dot{\Omega}$ (ergs s^{-1})	...	8.4×10^{31}
Magnetic field strength, B (G)	...	9.5×10^{11}
Spin-down age, $\tau = P/(2\dot{P})$ (yr)	...	1.4×10^7

J1908+0457 is the source of the X-rays since its derived spin-down luminosity $\dot{E} \sim 8.4 \times 10^{31}$ ergs s^{-1} is smaller than the observed luminosity of the IPC source (assuming a distance of 10 kpc) $L_X \sim 1.5 \times 10^{33}$ ergs s^{-1}. The other pulsar in the beam, B1905+04, is about 4'.5 from the X-ray source and is clearly not associated with it.

The pulse profile (Fig. 8*b*) suggests that pulse broadening from scattering has occurred. Again using the Cordes et al. (1994) parabolic fit, we estimate that for its DM, the expected timescale for scattering should be about 50 ms, or about 6% of the period. In Figure 8*b*, this value corresponds to 20° in pulse phase, which seems well fitted to the exponential tail observed.

6. DISCUSSION

The observed X-ray luminosities for all known (as of 1994 May) rotation-driven X-ray–emitting pulsars are plotted versus their spin-down luminosities in Figure 9. Different symbols denote the four different types of X-ray–emitting neutron stars ("Crab," "Vela," "Intermediate-age" and "old"). In this plot, we underlined the names of those for which no X-ray *pulsations* have been detected. The location of J0631+10 in this plot together with its spin-down age of 43 kyr are consistent with the other "intermediate-age" pulsars.

The fact that this pulsar is relatively young, suggests that some (if not all) of the observed X-ray emission may be due to an associated supernova remnant (SNR) since most SNR will disperse within approximately 10^5 yr. If indeed the hydrogen column density towards J0631+10 is approximately 10^{22} cm^{-2}, it is unlikely that the soft X-rays from an old SNR would be detected. The *Einstein* source 2E 1676 is slightly elongated (Fig. 4*a*), but no obvious diffuse emission is observed. On the other hand, the *ROSAT* source (Fig. 4*b*) has a small and faint extended companion source at approximately 2' away, which could be evidence of a supernova remnant. We are presently reducing infrared and VLA radio data in search of such a remnant. The closest known remnant is the Monogem ring, but with its center approximately 4° away from J9631+10, an association is not possible, given that the pulsar is only 43,000 yr old. This SNR was once believed to be associated with B0656+14 (Córdova et al. 1989), but later measurements of this pulsar's velocity imply that any neutron star resulting from that explosion is still to be found.

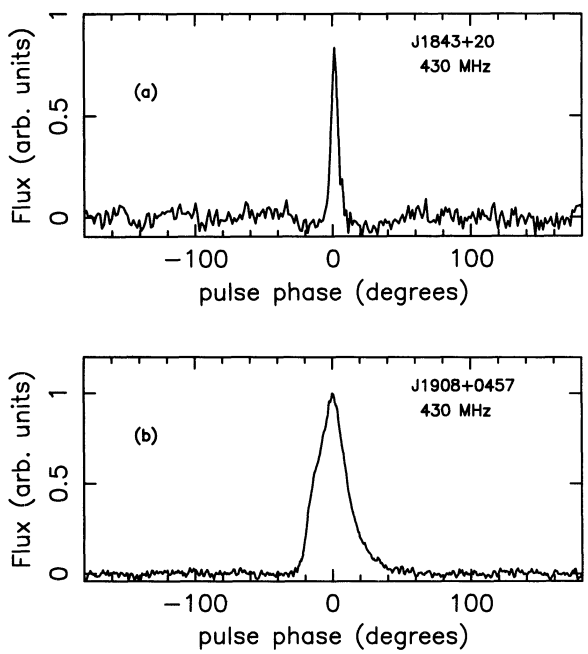

FIG. 8.—Average pulse profiles at 430 MHz for (*a*) J1843+20 and (*b*) J1908+0457.

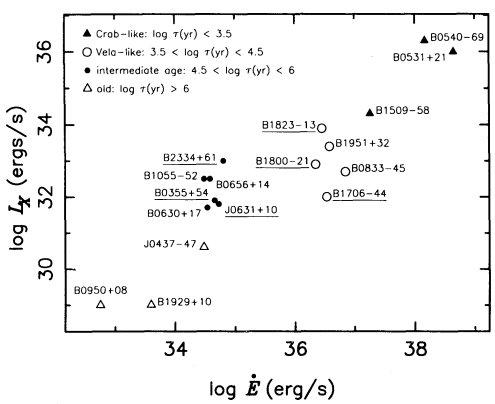

FIG. 9.—Plot of the X-ray flux vs. spin-down luminosity $\dot{E}$ for all known X-ray–emitting isolated neutron stars (as of 1994 May). Pulsars with underlined names have shown no detectable X-ray pulsation so far. Different symbols are used for the different "types" of X-ray–emitting neutron stars, which correlate with their spin-down ages.

Had the exposure time for 2E 1676 been 1 hr instead of 3 hr, this X-ray source would have S/N < 3.5; therefore, it would not have been included in the EOSCAT catalog. We thus believe that other X-ray–emitting pulsars remain undiscovered because their X-ray counterparts have not been detected owing to the increased absorption in the Galactic plane. In order to estimate this number, we compared the distribution of X-ray sources at low and high Galactic latitudes in the EOSCAT. Any deficiency of faint sources in the low Galactic latitude distribution is mostly due to the increased absorption because the stellar content in this distribution is relatively independent of Galactic latitude, since most of the X-ray–emitting stars are nearby and thus isotropically distributed. To compare the distributions at different Galactic latitudes, we normalized them to a single number of bright sources (count rate greater than 10 × the mean value) per steradian. We found that with this normalization, the number of faint sources at $|b| > 20°$ is about 50% higher than at $|b| < 5°$. This means that for every 100 sources found in the Galactic plane, about 50 others go undetected because of the increase in N_H. Therefore, given that from 520 sources found in the EOSCAT with $|b| < 5°$, seven are radio pulsars, we expect that the X-ray emission from three to four others was absorbed beyond the threshold of detection of the IPC detector.

The presence of an X-ray source at the location of J0631 + 10 both in the *Einstein* and *ROSAT* data is encouraging, though the positional errors are still too large to conclude that the pulsar and X-ray source are associated. The most direct way to confirm that J0631 + 10 is the X-ray emitter 2E 1676 would be to detect X-ray modulations at the radio period. A deep on-axis exposure maximizing sensitivity and without instrumental complications (such as rib shadowing) is needed to improve the preliminary X-ray position and spectrum. Currently, the only X-ray telescope capable of detecting J0631 + 10 is *ASCA*. Because of the seemingly harder spectrum for the X-ray source and the strong absorption of the soft X-ray emission, we expect a future *ASCA* observation of J0631 + 10 to answer decisively the issue of the existence and nature of the X-ray emission from this pulsar.

We thank D. Burrows and J. Mendenhall (Penn State University) for kindly providing us with their *ROSAT* exposure containing J0631 + 10. We are much in debt to F. Camilo (Princeton) and D. Nice (NRAO) for their quick derivation of the timing parameters of J1908 + 0457 and pulse profile by reprocessing their B1905 + 04 data. J. Fierro (Stanford) has kindly made available to us his software package *pulsar* for timing analysis of EGRET data. D. Harris (SAO) has provided valuable advice on the *Einstein* IPC data. W. Roberts (SAO) has helped in installing PROS in our local computer system. This work has been done under the NSF grant AST 9218075 and NASA grants NAG 5-1247, 5-1452, and 5-2436. I. W. acknowledges support from NASA grant NAGW-666 and NSF grants 93-15375 and 91-19475. This work was also supported by the National Astronomy and Ionosphere Center, which operates the Arecibo Observatory under a cooperative agreement with the National Science Foundation.

REFERENCES

Becker, W., & Trümper, J. 1993, Nature, 365, 528
Blaskiewicz, M., Cordes, J. M., & Wasserman, I. 1991, ApJ, 370, 643
Camilo, F. 1994, in The Lives of Neutron Stars, NATO ASI Ser., ed. M. Alpar, U. Kiziloghi, & J. van Paradijs (Dordrecht: Reidel),
Cordes, J. M., Romani, R. W., & Lundgren, S. C. 1993, Nature, 362, 133
Cordes, J. M., Spangler, S. R., & Weisberg, J. M. 1995, in preparation
Côrdova, F. A., Hjellming, R. M., Mason, K. O., & Middleditch, J. 1989, ApJ, 345, 451
De Jager, O. C., Raubenheimer, B. C., & Swanepoel, J. W. H. 1989, A&A, 221, 180
Foster, R. S., Wolszczan, A., & Cadwell, B. J. 1994, in Millisecond Pulsars: A Decade of Surprise, ed. A. Fruchter, M. Tavani, & D. Backer (San Francisco: ASP), 24
Frail, D. A., Kulkarni, S. R., & Vasisht, G. 1993, Nature, 365, 136
Fruchter, A. S. 1989, Ph.D. thesis, Princeton Univ.
Fruchter, A. S., Bookbinder, J., Garcia, M. R., & Baylin, C. D. 1992, Nature, 359, 303
Hassinger, G., Boese, G., Predehl, P., Turner, T. J., Yusaf, R., Geroge, I. M., & Rohrbach, G. 1993, MPE/OGIP Calibration Memo CAL/ROS/93-015
Harris, D., et al. 1990, The *Einstein Observatory* Catalog of IPC X-Ray Sources (Cambridge: Smithsonian Astrophysical Obs.)
Hester, J. J., & Kulkarni, S. 1988, ApJ, 331, L121
Johnston, S., et al. 1992, ApJ, 387, L37
Kulkarni, S., & Heiles, C. 1988, in Galactic and Extragalactic Astronomy, ed. G. L. Vershuur & K. I. Kellermana (2d ed.; Berlin: Springer)
Kulkarni, S., & Hester, J. J. 1988, Nature, 335, 801
Kulkarni, S. R., Phinney, E. S., Evans, C. R., & Hasinger, G. 1992, Nature, 359, 6393
Lynds, B. T. 1962, ApJS, 7, 1
Manchester, R. N. 1974, ApJ, 188, 637
Manchester, R. N., & Taylor, J. H. 1977, Pulsars (New York: Freeman)
Nice, D. J. 1994, in Millisecond Pulsars: A Decade of Surprise, ed. D. Backer, A. Fruchter, & M. Tavani (San Francisco: ASP), 9
Ögelman, H. 1994, in The Lives of Neutron Stars, NATO ASI Ser., ed. M. Alpar, U. Kiziloghi, & J. van Paradijs (Dordrecht: Reidel), in press
Phinney, E. S., & Kulkarni, S. R. 1994, ARA&A, 32, 591
Shevchenko, V. S., & Yabukov, S. D. 1988, Soviet Astron., 32, 484
Taylor, J. H., & Cordes, J. M. 1993, ApJ, 411, 674 (TC93)
Taylor, J. H., & Weisberg, J. M. 1989, ApJ, 345, 434
Wang, Q. D., Li, Z.-Y., & Begelman, M. 1993, Nature, submitted
Weisberg, J. M. 1978, Ph.D. thesis, Univ. of Iowa
Zepka, A. F., Cordes, J. M., & Wasserman, I. 1994, ApJ, 427, 438